CHAPTER 14

Cellular Magnetic Labeling with Iron Oxide Nanoparticles

SÉBASTIEN BOUTRY, SOPHIE LAURENT, LUCE VANDER ELST, and ROBERT N. MULLER

Department of General, Organic and Biomedical Chemistry, NMR and Molecular Imaging Laboratory, University of Mons, Mons, Belgium

14.1 INTRODUCTION

For molecular magnetic resonance imaging (MRI), an amplification of the molecular labeling is required. This can be achieved, for example, by avidin–biotin systems in the extracellular compartment [1]. Cellular internalization of the contrast agent is a way to increase the labeling of targeted cells. The challenge for cellular MRI is obtaining a sufficient uptake of MRI contrast agents in cells, especially nonphagocytic cells, in order to render them distinct from the surrounding tissue. Although this approach gives less specific results than molecular MRI, it offers suitable systems for the noninvasive and repeated *in vivo* monitoring (identification and tracking) of cells by MRI. Magnetic labeling can be realized *in vitro* or *in vivo* through specific (involving a cell surface receptor) or nonspecific cellular internalization pathways with contrast agents considered as positive (complexes of paramagnetic ions such as gadolinium(III) or manganese(II); shortening the T1 of their adjacent hydrogen nuclei as a predominant effect and brightening the regions taking them up on a T1-weighted MR image), and often with contrast agents considered as negative (superparamagnetic particles based on a monocrystalline or polycrystalline iron oxide core, shortening the T2 and $T2^*$ much more than the T1 of hydrogen nuclei in their neighborhood and generating a signal darkening on T2 ($T2^*$)-weighted MR images). Many studies have indeed been performed *in vitro* and *in vivo* with iron oxide nanoparticles [2, 3]. Another mandatory point about cellular MRI is that the loading of cells with contrast agents does not have to affect normal cell function [3]. This chapter mainly focuses on the use of native (unmodified) or unspecifically cell-targeted iron oxides as cell markers. Some examples of cellular labeling performed with other MRI contrast agents, or obtained via specific internalization pathways, are also given.

Nanoplatform-Based Molecular Imaging Edited by Xiaoyuan Chen

14.2 SPECIFIC MAGNETIC LABELING OF CELLS

This type of magnetic labeling occurs via receptor-mediated endocytosis (Fig. 14.1), which is a highly specific and efficient mechanism of internalization. The transferrin receptor (TfR) pathway has been used to label cells in several studies. Transferrin (Tf), an iron chelating protein, interacts with TfR and enters cells by receptor-mediated endocytosis, supplying them with iron from stores in the liver. As iron is an essential element involved in cell proliferation, a high number of TfRs is expressed in proliferating cells [4]. Thus, this mechanism of iron uptake appears as an interesting marker for tumor cells, or an interesting way to label progenitor cells. Furthermore, the high turnover rate of the TfR avoids the phenomenon of receptor saturation [5]. Oligodendrocyte progenitors (CG-4) have been magnetically labeled in culture with monocrystalline iron oxide nanocompound (MION) covalently linked to an antibody (OX-26) specific for TfR. The binding of OX-26 to TfR induced the internalization of the nanoparticles. Labeled cells were tracked by MRI after transplantation into the spinal cord of myelin-deficient rats and were found to synthesize myelin [6].

In another study, the *in vitro* receptor-mediated endocytosis of Tf covalently linked to ultrasmall superparamagnetic iron oxide (USPIO) (Tf-USPIO) by human epidermoid carcinoma A431 was observed. Tf-USPIO was also injected intravenously (200 μmol Fe/kg) into rats bearing implanted mammary carcinoma. Despite the fact that most of the injected dose was captured by the liver and the spleen, MR imaging results showed a signal reduction in the tumor only with Tf-USPIO and not with the parent compound or a nonspecific albumin-bound USPIO, suggesting a transferrin-mediated endocytosis of USPIO by the tumor [5]. In another approach, rat 9L gliosarcoma cells were transfected with a modified gene coding for the human TfR, to constitutively express high levels of the receptor protein. The engineered cells were implanted in mice flank and a strong negative contrast was detected in the resulting tumors after intravenous injection of MION conjugated to human holo-transferrin (Tf-MION) (3 mg Fe/animal). This result suggested an efficient uptake of Tf-MION by tumor cells and provided the possibility to image transgene expression [7]. The approach, consisting of the manipulation of iron metabolism genes to provide cellular iron accumulation and subsequent MRI contrast, was further developed in a study where coexpression of transgenic human TfR and human ferritin H-subunit was induced in a stably transfected neural stem cell line (C17) [8]. Ferritin (FT) is composed of H- and L-subunits. Twenty-four subunits form the apoferritin, which is able to incorporate up to 4500 iron atoms. The H-subunit has a ferroxidase activity that promotes iron oxidation and incorporation [9, 10]. Thus FT-bound iron has a semicrystalline structure and acts as an endogenous cellular negative contrast agent. These studies demonstrated that transfected cells grown in iron-rich medium incorporated significantly more iron than control cells, inducing a contrast effect in MRI that was preserved after transplantation

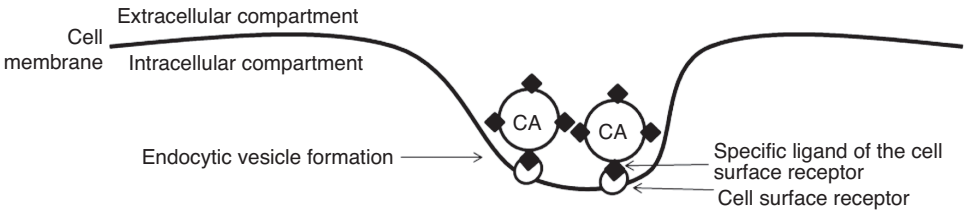

FIGURE 14.1 Schematic representation of the receptor-mediated endocytosis of a contrast agent (CA).

of cells into the mouse brain. After uptake through TfR, iron was stored by FT without affecting cell viability [8]. The usefulness of FT as an endogenous contrast agent has been reported also after inducing the overexpression of this protein by C6 rat glioma cells. Indeed, intracellular iron is redistributed in excess FT, which generates negative contrast. As iron chelation induces a transient decrease of intracellular iron concentration, TfR is expressed in compensation to increase the iron uptake and restore iron homeostasis. This newly endocytosed iron will also be sequestered by overexpressed FT, leading to an enhancement of the contrast effect [11].

The internalization pathway of a vitamin has also been used often to shuttle iron oxides in cells. The folate (or vitamin B_9) receptor has been targeted with folic acid-linked MRI contrast agents in order to induce an uptake of the cell tag by cancer cells overexpressing the receptor [12]. The internalization of superparamagnetic nanoparticles bearing chlorotoxin in the cytoplasm of 9L glioma cells has been reported. This 36 amino acid peptide indeed renders the nanoprobe capable of targeting tumor cells expressing membrane-bound matrix metalloproteinase-2 [13]. Prostate cancer cells could be labeled via receptor-mediated endocytosis with iron oxides conjugated to an antibody specific for the prostate-specific membrane antigen (PSMA) [14]. Intracellular accumulation of iron oxide nanoparticles in cells has been achieved also by targeting hormone receptors. The single chain anti-epidermal growth factor receptor (EGFR) antibody has been bound to iron oxide nanoparticles to serve as an intracellular marker of EGFR-expressing cancer cells [15]. Luteinizing hormone releasing hormone (LHRH) and luteinizing hormone/chorionic gonadotropin (LH/CG)-conjugated iron oxide nanoprobes have been used to label breast cancer cells [16].

14.3 NONSPECIFIC MAGNETIC LABELING OF CELLS

This type of magnetic labeling can occur via natural mechanisms of endocytosis, which are not receptor dependent. In this context of nonspecific magnetic labeling of cells, most of the studies concern the *in vitro* labeling of nonphagocytic cells potentially useful for cell therapy. Among these cells of interest we find mesenchymal cells, embryonic stem cells, neural stem cells, oligodendrocyte progenitor cells, endothelial progenitor cells, and muscle progenitor cells. In other words, undifferentiated or less differentiated cells that, after their reintroduction in a living organism, could hopefully reach the damaged area (ischemic lesion) of an organ and differentiate to replace dead cells or, more specifically for endothelial precursors, reach a tumor were angiogenesis is occurring. Many *in vitro* cellular magnetic labeling studies are performed also on $CD34^+$ hematopoietic stem cells or immune cells (lymphocytes) because the study of their *in vivo* trafficking could help us to better understand the immune response and, more particularly, to improve cell-based cancer therapies [2, 3, 17]. Thus visualization of the *in vivo* behavior of these cells is crucial and depends on their prelabeling in culture. Furthermore, the study of contrast agent accumulation in phagocytes and tumor cells can become a tool for the biological characterization of pathologies [18, 19].

14.3.1 Fluid-Phase Endocytosis of Contrast Agents With or Without the Help of a Transfection Agent: Influence of the Contrast Agent Surface Charge

Gadolinium-based contrast agents have been developed for the *in vitro* labeling of cells. Gd chelates coupled to fluorescent rhodamine dextran (GRID), or the combined use of Gd

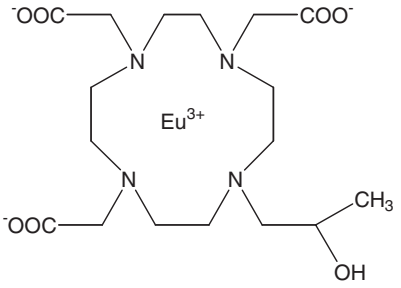

FIGURE 14.2 Structure of Eu-HP-DO3A.

and europium (Eu, fluorescent) complexed by the chelate HP-DO3A (ProHance®, Bracco Diagnostics, Milan, Italy) (Fig. 14.2), constitute bimodal agents. Indeed, the detection of reimplanted labeled cells can be achieved by *in vivo* MRI and corroborated by fluorescent histology [3, 20, 21].

Lanthanide ions such as Eu(III) or terbium(III) (Tb(III)) have been used to build complexes called paramagnetic chemical exchange saturation transfer (PARACEST) agents. When the mobile (exchangeable) protons of these complexes are irradiated at their absorption (resonance) frequency, they transfer saturated magnetization to the surrounding bulk water, acting so as negative contrast agents. Thus contrast alteration on MR images is based on a phenomenon called chemical exchange dependent saturation transfer (CEST). As the resonance frequency of the exchangeable protons of the complex is influenced differently according to the type of paramagnetic ion used, PARACEST agents can generate their own specific contrast when irradiated at the specific absorption frequency of their mobile protons. In other words, cells labeled *in vitro* with different PARACEST agents, by internalization of the complex through pinocytosis, could be distinguished and separately tracked *in vivo* (Fig. 14.3a) [22]. Several attempts have been made to improve the *in vitro* cellular uptake of Gd chelates. Gd-DTPA has been combined with transfection agents such as calcium phosphate or the lipofection agent Lipofectamine™, usually facilitating the delivery of functional DNA into the cell [23].

Unmodified dextran-coated iron oxide nanoparticles can be used to label cells *in vitro*. Lymphocytes or T cells in culture have been loaded with this type of contrast agent through fluid-phase endocytosis [24, 25]. Rat bone marrow mesenchymal cells and mouse

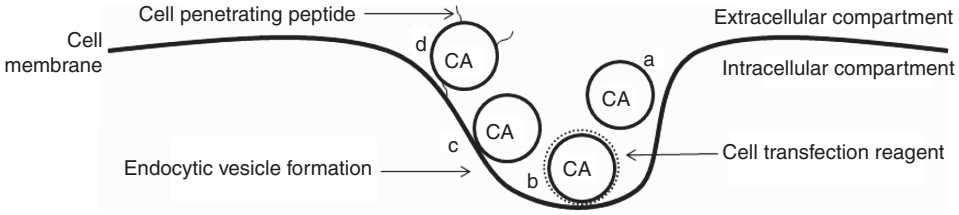

FIGURE 14.3 Schematic representation of the uptake of contrast agents (CAs) by cells through nonspecific (receptor-independent) endocytic processes: (a) fluid-phase endocytosis (pinocytosis) of the native CA, (b) endocytosis after adsorption of the CA mixed with a cell transfection reagent to the cell surface, (c) endocytosis after adsorption of the native CA to the cell surface, and (d) endocytosis after adsorption of a "cell penetrating peptide"-conjugated CA conjugated to the cell surface.

embryonic stem cells were simply incubated with superparamagnetic iron oxide (SPIO) (Endorem®) at a relatively high concentration (around 100 μg Fe/mL in the cell culture medium for 48–72 h of incubation) [26–29]. In both cases, the *in vivo* fate of labeled cells was successfully MR imaged *in vivo*. However, in many studies, the cellular uptake of SPIO (Feridex®) is optimized by mixing the superparamagnetic contrast agent with a cationic transfection agent such as poly-L-lysine. It is hypothesized that these dextran-coated SPIO nanoparticles can be coated with the positively charged transfection agent through electrostatic interactions. The citrate-containing formulation of Feridex® (or Endorem®) may allow for the presence of a few carboxyl groups at the particle surface, which was indeed found to be negatively charged (zeta potential of -41 mV for Feridex®) [30, 31]. Thanks to the positive charges of poly-L-lysine, the complex rapidly binds to the negatively charged cell membrane and is shuttled into cells through endosomes, producing a cellular magnetic labeling equivalent to the loading obtained by simply adding SPIO to the culture medium of cells (10–20 pg Fe/cell). However, the iron incubation concentration is lower (25 μg Fe/mL (vs. ~100 μg Fe/mL)) and the magnetic labeling duration can potentially be shorter (2–48 h, depending on the cell type (vs. 48–72 h)). In the case of human mesenchymal stem cells, an iron content of 16 pg/cell has been found after a 2-h incubation [3, 32, 33]. The same approach has been developed with other commercial transfection agents, which have been combined with iron oxide nanoparticles in order to form complexes possessing a net positive charge that can associate with the negatively charged cell surface [34]. The resulting increase of contrast agent uptake has allowed for an improvement of the magnetic labeling of cultured cells.

Another polycationic amine, protamine sulfate (Food and Drug Administration approved), has been used instead of poly-L-lysine to form complexes with SPIO (Feridex®) and label human mesenchymal stem cells or $CD34^+$ cells [35]. Superfect™ consists of activated dendrimers with a spherical architecture and branches radiating from a central core and terminated by positively charged amino groups [36]. This commercially available transfection reagent has also been suitable for the magnetic labeling of mammalian cells with SPIO (Feridex®). An iron content of 30 pg Fe/cell has been obtained for human mesenchymal stem cells incubated for 2 h with the Superfect™–Feridex® complex (25 μg Fe/mL), a value twice higher than with poly-L-lysine–Feridex® complex under the same conditions [33, 35]. The mechanisms initiating the endocytosis of dendrimers and polyamine-complexed iron oxide nanoparticles are thought to be of an electrostatic origin. Indeed, the adsorption of the positively charged complex on the negatively charged cell surface is supposed to induce membrane bending and membrane disruption. These phenomena induce invaginations of the cell membrane, leading to the encapsulation of the complexes in endosomes (Fig. 14.3b) [3, 32].

A carboxylated dendrimer has also been used as a coating for iron oxide nanoparticles. The carboxylate groups gave an anionic surface to the dendrimers. The resulting magnetodendrimer, called MD-100 (Fig. 14.4), has successfully served as a magnetic marker for different cultured cell types, originating from mouse, rat, and human, including stem cells. The uptake mechanism of MD-100 is also believed to result from electrostatic interactions between the dendrimer and the cell surface. The highly charged polymers bind on multiple sites on the cell membrane, inducing bending and disruption of the plasma membrane. An amount of 9 pg Fe/cell has been reached for CG-4 rat oligodendrocyte progenitors after 48 hours of incubation with MD-100 (25 μg Fe/mL) [3, 37, 38]. A binding of nanoparticles bearing negative charges to the cell surface, which is also mainly negatively charged, appears as contradictory, and the reason for such an event is unknown. Nevertheless, a high level of

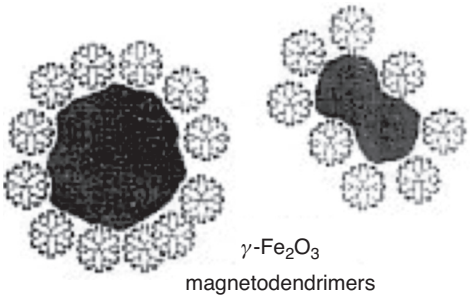

FIGURE 14.4 Structure of magnetodendrimers (adapted from [32]).

cell internalization, comparable to the one obtained with the magnetodendrimer MD-100, has been obtained also with anionic iron oxide nanoparticles. The negative surface charge of these nanoparticles, due to the unbound carboxylate groups of their dimercaptosuccinic acid coating, has been hypothesized to allow them to interact strongly and nonspecifically with cationic sites of the plasma membrane, which are much more scarcely distributed than anionic areas. This mechanism involving an adsorption of the nanoparticles on the cell surface through electrostatic interactions, preceding their internalization, is called adsorptive endocytosis (Fig. 14.3c) [39].

Commercially available anionic nanoparticles (carboxydextran-coated SPIO (Resovist®)) have been found to be more efficient than dextran-coated SPIO (Feridex®) to label cultured cells. Furthermore, the effectiveness of the intracellular uptake of nanoparticles has been found to be dependent on the density of carboxyl groups at the nanoparticle surface (with there being an optimum density), as well as on the cell type. The uptake of anionic nanoparticles has indeed been observed to be more pronounced in mesenchymal stem cells than in human cervical carcinoma (HeLa) cells, and a lower density of carboxyl groups was necessary to obtain an effective uptake of nanoparticles by mesenchymal stem cells compared to the latter cancer cells. Indeed, Feridex® was captured in a higher amount by mesenchymal stem cells than by HeLa cells. It was hypothesized that the citrate used in the preparation of Feridex® might allow for the presence of a few carboxyl groups at the surface of nanoparticles, which would be sufficient to trigger an uptake of Feridex® by mesenchymal stem cells, but not by HeLa cells [30]. The magnetic labeling of cultured nonphagocytic adherent cells with iron oxide nanoparticles has been found to be dependent on the relative concentration of the magnetic tag and of the cells in culture, on the nanoparticle hydrodynamic diameter, and on the coating charge (Fig. 14.5) [40].

14.3.2 Cellular Delivery of Contrast Agents by Cationic Liposomes

The same approach as for dendrimers and polyamines has been developed with liposomal transfection reagents [34]. Several types of superparamagnetic iron oxide nanoparticles, including Feridex®, Endorem®, Sinerem® (dextran-coated), or P7228 (covered by an anionic dextran derivative), have been incorporated into cationic transfection liposomes (such as Lipofectamine™ or FuGENE™). The lipid complex, carrying a net positive charge, binds to the negatively charged cell surface (Fig. 14.3b). The delivery of the contrast agent to the cytoplasm then depends on the liposome–cell membrane fusion. It has been demonstrated that this fusion only occurred after uptake of the liposome into the endocytic

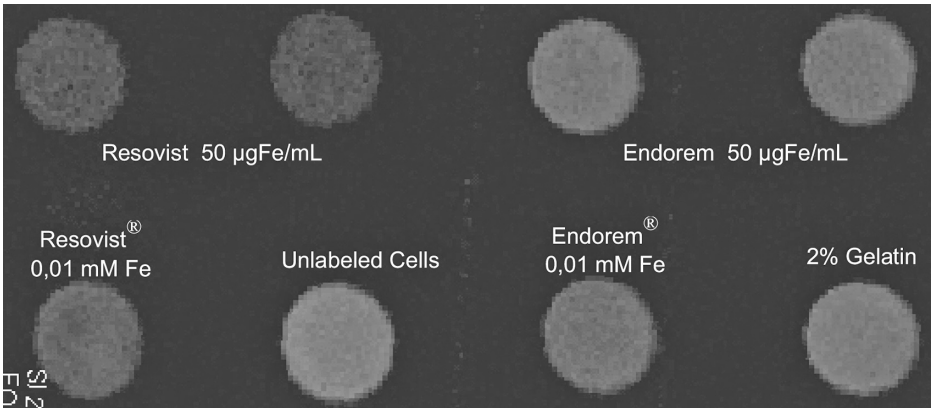

FIGURE 14.5 T2-weighted MR images (TR/TE: 3000/15 ms, 16th echo (240 ms), 5×10^5 cells/mL in 2% gelatin) of 3T6 fibroblasts, after 48 h of SPIO labeling with 50 µg Fe/mL of Endorem® or Resovist® (upper row samples). Samples imaged on the bottom row (from left to right: Resovist® nanoparticles at 0.01 mM Fe, unlabeled cells, Endorem® at 0.01 mM Fe, and 2% gelatin) are for comparison (from [40]).

pathway [41]. These cationic liposome–iron oxide nanoparticle complexes have been used to magnetically label several types of mammalian cells including mouse embryonic stem cells, human mesenchymal stem cells, rat oligodendrocyte progenitor CG-4 cells, rabbit skeletal myoblasts, human hematopoietic progenitor cells, mouse lymphocytes, or HeLa cells [29, 33, 42, 43]. The iron content of human mesenchymal stem cells was 7.6 pg/cell after a 2-h incubation with 25 µg Fe/mL of Lipofectamine™–Feridex® complex. In other terms, this loading was twice lower than with the poly-L-lysine-Feridex® complex used under the same conditions [33].

14.3.3 Cellular Delivery of Contrast Agents Through a Cell Penetrating Peptide

Another nonspecific way of cellular internalization exists, since some natural proteins, such as the human immunodeficiency virus (HIV) Tat (transactivator of transcription) protein, have the ability to penetrate cell membranes directly. The basic domain of the HIV Tat protein, formed of an arginine-rich sequence, has been identified as the domain responsible for the translocation of this protein. The highly cationic peptide derived from this basic domain is called a cell-penetrating peptide because of its ability to cross the plasma membrane and consequently to drag the rest of the protein with it [44, 45]. The mechanism by which this task is performed is based on an interaction of the peptide with glycosaminoglycans attached to cell surface heparan sulfate proteoglycans, initiating an adsorptive endocytic process (Fig. 14.3d) [46, 47]. Gd chelates and iron oxide nanoparticles have been conjugated to the Tat basic domain peptide (or more simply, Tat peptide) in order to efficiently transport the contrast agents into cells. Mammalian cells have been labeled successfully with Tat peptide-derivatized Gd-DOTA,[48, 49] or superparamagnetic contrast agents linked to the Tat peptide [50–52]. Human $CD34^+$ hematopoietic stem cells labeled for 1 h with the Tat peptide-conjugated iron oxide nanoparticles (100 µg Fe/mL) contained from 10 up to 30 pg Fe/cell [50].

14.3.4 Instant Cellular Delivery of Contrast Agents by Electroporation

This method, called magnetoelectroporation (MEP), circumvents a prolonged incubation of cells and the use of a transfection agent, and allows achieving an instant magnetic labeling of cells. Mesenchymal stem cells and neural stem cells have been labeled with SPIO (Feridex®) by the MEP method. The nanoparticles were taken up in endosomes and the iron content of cells (picogram range/cell) was comparable to values obtained with transfection agents. Furthermore, when used under properly calibrated conditions (a pulse of 130 V for 17 ms), MEP is claimed to have no effect on cell viability, proliferation, or differentiation [53].

14.3.5 Fluid-Phase Endocytosis of Contrast Agents with Micron-Sized Particles

Some advantages have been found in the use of micrometer-sized particles of iron oxide (MPIO) to label cells, as compared to the dextran-coated iron oxide nanoparticles SPIO or USPIO. For the latter, the endocytosis of millions of nanometer-sized particles is required to achieve sufficient contrast, and cell division can dilute the label beyond the detection threshold. MPIO (Bangs Laboratories, Fishers, Indiana, USA) are magnetite cores encapsulated with styrene/divinyl benzene. Various sizes exist (from 0.76 to 5.80 μm in diameter). The smallest ones (0.76–1.63 nm) also contain a fluorescein-5-isothiocyanate analog (Dragon Green). Human $CD34^+$ hematopoietic progenitor cells and porcine mesenchymal stem cells have been reported to efficiently internalize 0.9-μm MPIO through endocytosis under incubation conditions (concentration and duration) comparable to those used with dextran-coated nanoparticles (e.g., 18 h with 45.6 μg Fe/mL), and to lead to an iron load of hundreds of picograms per cell [54]. The styrene/divinyl benzene coating is thought to be inert inside cells and cannot be degraded within the cell, which is not the case with the dextran coating [55]. As the $T2^*$ effect of an iron oxide particle increases with its size, these MPIO have a larger $T2^*$ effect than SPIO in MRI, making possible the detection of single particles by *in vitro* MRI with a 50-μm resolution in agarose phantoms or in cultured cells [56]. The possibility to MR image labeled cells by detecting single endocytosed particles overcomes the problems related to the dilution of the magnetic label induced by cell divisions [57]. Furthermore, it has been shown that mouse hepatocytes, prelabeled with 1.63-μm MPIO, were detectable by MRI as single cells in the liver of recipient mice 1 month after their transplantation into the spleen [58].

14.4 MAGNETIC LABELING OF PHAGOCYTES

It has been demonstrated that dextran-coated SPIO (Endorem®) undergo a higher macrophage uptake than the smaller-sized dextran-coated USPIO (Sinerem®) *in vitro*, confirming their respective *in vivo* biodistribution; SPIO are rapidly cleared from the circulation as a result of their capture mainly by liver Kuppfer cells, and USPIO have a longer blood half-life, allowing them to reach macrophages situated in less accessible territories, such as lymph nodes [59].

Scavenger receptors (SRs) are relatively nonspecific receptors mainly expressed by macrophages. These receptors bind to a broad range of negatively charged macromolecules (class A) or modified low-density lipoprotein (LDL) (class A and class B). The class A SR

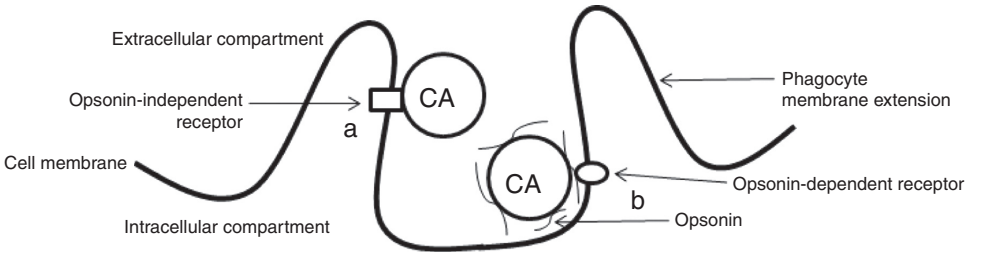

FIGURE 14.6 Schematic representation of the uptake of MRI contrast agents (CAs) by phagocytic cells: (a) endocytosis initiated by a receptor mediating an opsonin-independent recognition of the CA as a phagocytic target, and (b) endocytosis initiated by a receptor mediating a recognition of the CA as a phagocytic target through opsonins adsorbed to its surface.

(SR-A) types I and II bind anionic proteins, lipids, polynucleotides, and polysaccharides including dextran sulfate or fucose sulfate (fucoidan) and bacterial lipopolysaccharides [59]. The SR-A types mediate an opsonin-independent recognition of microorganisms or apoptotic cells before their phagocytosis (Fig. 14.6a) [60]. Competition experiments have suggested that the endocytosis of SPIO by cultured macrophages was mediated by the SR-A types. Indeed, ligands of the SR-A (fucose sulfate and polyinosinic acid) were effective inhibitors of the SPIO capture by cultured mouse peritoneal macrophages [59]. Phagocytosis concerns the uptake by macrophages of large material, such as bacteria ($\sim$1 μm) or senescent eukaryotic cells ($\sim$10 μm), which are much larger than the hydrodynamic diameter of iron oxide nanoparticles. The larger-sized dextran-coated SPIO (80–150 nm) can nevertheless initiate their macrophage endocytosis by interacting with the SR-A [59]. The macrophage uptake of dextran-coated USPIO (20–40 nm) occurs primarily through a pinocytosis mechanism and leads to a weaker internalization of nanoparticles than with dextran-coated SPIO [59, 61]. However, it has been demonstrated that citrate-coated very small superparamagnetic iron oxide nanoparticles with a hydrodynamic diameter of 8 nm (VSOP-C125) were efficiently taken up by macrophages through a mechanism involving actin, which is the cytoskeleton component determinant for phagocytosis. This result suggests that the pronounced negative surface charge of the nanoparticles could help their macrophage endocytosis by allowing an interaction with a receptor initiating phagocytosis. Another important point in this context is that the clustering of the nanoparticles, leading to the formation of larger-sized particulate aggregates, can also result in different uptake stimuli for macrophages (i.e., phagocytosis rather than pinocytosis) [61]. Particles can also bind to nonspecific scavenger receptors after adsorption to their surface of proteins from the heat-inactivated fetal bovine serum supplement added in culture medium [62].

In fresh plasma, MION have been covered by vitronectin, by fibronectin, and by fragments of the complement fraction C3 (C3b and its fragment C3dg) bound to IgG heavy or light chain [18]. This opsonization induced the recognition of MION by specific receptors on the macrophages (Fig. 14.6b) [63]. Indeed, IgG heavy chain-complexed dimeric forms of C3b and C3dg are ligands for the complement receptors CR1 and CR2, respectively [64]. The vitronectin receptor and the β2 integrins, such as the complement receptors CR3 and CR4, usually bind the opsonin iC3b (fragment of C3b). They can also mediate the nonopsonic recognition of phagocytic targets [60, 63]. Iron oxide nanoparticles have been targeted to a β2 integrin for the *in vitro* magnetic labeling of dendritic cells before their reimplantation and *in vivo* MRI monitoring. By conjugation to an antibody, iron oxide nanoparticles

have been targeted to CD11c, the alpha subunit of the β2 integrin CR4 (CD11c/CD18), and allowed to obtain an efficient intracellular labeling *in vitro* through receptor-mediated endocytosis [64]. Gd-based contrast agents (Gd-DTPA) have been linked to long fatty acid chains in order to form 0.5–1-μm insoluble particles. These foreign particles were captured by dendritic cells *in vitro* through phagocytosis and intracellular lipases cleaved the long aliphatic side chains, restoring the solubility of Gd-DTPA and consequently its contrast agent activity inside the cells [65].

14.5 TOXICITY

From the toxicity point of view, iron oxides are generally well tolerated by cells. No significant short-term toxicity of iron oxide nanoparticles has been reported [3, 26, 33, 37, 42]. Several studies have shown that the endosomal incorporation of iron oxide nanoparticles did not affect cell viability or proliferation, but it was found that Feridex® complexed to poly-L-lysine had an effect on the human mesenchymal stem cells' differentiation into chondrocytes [66]. Furthermore, the same complex significantly affected the viability of marrow stromal cells as compared to unlabeled control cells when incubations were done for long periods (24 or 72 h) with relatively high concentrations (100 and 250 μg Fe/mL). On the contrary, a labeling with Feridex®–poly-L-lysine complexes at 25 μg Fe/mL did not induce any significant mortality of mesenchymal stem cells, even after a 72-h incubation period, and long-term toxicity studies performed after a 16–18-h incubation period of mesenchymal stem cells with the same amount of complex did not show any significant cell death as compared to unlabeled control cells until 15 days postlabeling [67]. The metabolic fate of internalized iron has not been well determined in current studies. It is assumed that iron atoms are integrated in the normal iron turnover inside the cell [3]. Nonetheless, incubation with iron oxide at high concentrations (1 mgFe/mL for 24 h) has been found to cause the generation of free radicals, a decrease in proliferation, and cell death [43]. VSOP were massively taken up by macrophages and were reported to induce a transient oxidative stress in these cells [68]. Human neural precursor cells that were labeled for 72 h with Sinerem® (800 μgFe/mL) did not show any loss of short-term viability. However, a decrease in their subsequent survival and a reduction in their neurosphere-forming capacity were observed when cells were dissociated and plated in culture under standard growth conditions after incubation with the USPIO (more than 80% of cell death at the first subculturing passage postlabeling). This phenomenon was avoided with lower incubation concentrations (e.g., 400 μgFe/mL) and shorter incubation times (e.g., 48 h). Poly-L-lysine has been found to improve the labeling efficiency of both Sinerem® and Endorem® without impairing cell survival, even surprisingly increasing the short-term survival of the human neural precursor cells at high iron incubation doses (100 μgFe/mL for Endorem®, and 200 and 400 μgFe/mL for Sinerem®) [69]. Higher Sinerem® incubation concentrations (up to 22 mg Fe/mL) and a shorter incubation time (12 h) have been used to perform a cationic liposome (Metafectene®)-helped labeling of D3 embryonic stem cells [70]. Toxicity was mainly induced by the transfection agent (50% of immediate cell death at 25 μL Metafectene®/mL). A small influence of Sinerem® alone on cell proliferation was only observed at the highest iron incubation concentration. In the same study, comparisons between different cell lines (D3 embryonic stem cells, C17.2 neuronal progenitor cells, and dendritic cells) were also performed: just as the uptake of a given superparamagnetic cell tag is cell line specific, the tolerance to the transfection agent was also observed to be dependent on the cell type [70].

14.6 APPLICATIONS OF CELLULAR MAGNETIC LABELING WITH UNMODIFIED OR UNSPECIFICALLY CELL-TARGETED MRI CONTRAST AGENTS

The main application of cellular magnetic labeling is the *in vivo* tracking of cells by the noninvasive MRI technique, principally in the context of cell therapies. This method provides the possibility to visualize the migration of cells such as lymphocytes during the immune response. It also allows for the monitoring of the *in vivo* fate and behavior of cells (e.g., stem or progenitor cells) transfused in a diseased living organism, or directly transplanted in a damaged organ. Cellular imaging of phagocytes infiltrated in inflammatory areas has also been reported, as well as the magnetic labeling of tumors. In many studies, iron oxide nanoparticles have been chosen for cell labeling *in vitro* or *in vivo* and have been effective as magnetic tags to follow the cells *in vivo* by MRI [3].

14.6.1 MRI Monitoring of Cells Transplanted or Transfused *In Vivo* After *In Vitro* Magnetic Labeling

The *in vivo* distribution of magnetically labeled cells from the hematopoietic lineage has been studied by MRI. Hybridomas (a fusion between B lymphocytes and myeloma cells) internalized anionic nanoparticles *in vitro* and were intraperitoneally injected in the mouse. MRI suggested a homing of the labeled cells in the spleen 24 h postinjection. These cells were also found to proliferate in the spleen [71]. Magnetically labeled human hematopoietic progenitor cells were intravenously injected in athymic mice. MRI monitoring showed signal attenuations in spleen, liver, and bone marrow. Histology confirmed the homing of the labeled cells in these recipient organs [72]. Tat peptide-derivatized iron oxide nanoparticles have also been applied to image cell trafficking *in vivo* after intravenous injection of $CD34^+$ cells into immunodeficient mice. These cells, prelabeled with superparamagnetic–Tat peptide conjugates, were detected in the bone marrow by MRI [50]. The MRI tracking of prelabeled lymphocytes (T cells) has also been performed in the context of the mouse experimental autoimmune encephalomyelitis (EAE) model, allowing researchers to collect information about the pathogenesis of this dysmyelinating disease [73].

Because of its high relevance for immune cell-based anticancer therapies, the *in vivo* trafficking of tumor-targeted lymphocytes has been studied in several models. Iron oxide nanoparticles conjugated to a large number of Tat peptides were used to label $CD8^+$ cytotoxic T lymphocytes stimulated with the ovalbumin-derived immunogenic peptide. Ovalbumin-transfected B16 melanoma cells were subcutaneously implanted in mice and intraperitoneally injected with the labeled cells. The tumoral recruitment of these cells was visualized by MRI and confirmed by histological analysis [74]. In a similar type of animal model, ovalbumin-specific splenocytes, labeled with iron oxide nanoparticles, were injected into mice with ovalbumin-expressing tumors. MRI results suggested that cells went first to the spleen (homing, 24 h postinjection) before being recruited by the tumor (48–72 h postinjection) [75]. The *in vivo* MRI monitoring of the accumulation of immune cells in tumors was also reported in a study performed with human natural killer cells directed against HER2/neu receptors, expressed by mammary tumors. Cells were magnetically labeled with iron oxide nanoparticles and intravenously injected into mice bearing HER2/neu-positive mammary tumors. The tumoral signal decay in MRI, confirmed by histology results, demonstrated the presence of the labeled natural killer cells in the tumors [76]. These different reports have shown the usefulness of MRI as

a noninvasive method for the monitoring of cell-based immunotherapies. Furthermore, a human approach to therapeutic cell tracking appeared as clinically safe. Dendritic cells, which can play the role of an antitumor cellular vaccine since they are antigen-presenting cells, were SPIO-labeled and detected by MRI after injection in the lymph nodes of patients suffering from melanoma. MRI showed how accurate the nodal delivery was of the iron oxide-loaded autologous dendritic cells [77].

Many attempts of stem cell transplantation have been performed with the aim of repairing central nervous system (brain or spinal cord) disorders, and promoting anatomical and functional recovery. The magnetic prelabeling of these cells allows visualization of their presence and their migration by MRI. In order to provide a strategy of cell therapy to reverse dysmyelinating diseases, stem cell-derived oligodendrocyte progenitors (CG-4) were magnetically labeled and were observed to migrate after transplantation in the spinal cord of 7-day-old myelin deficient rats. Furthermore, histological analysis identified iron-loaded cells as oligodendrocytes, and detected newly formed myelin in areas corresponding to the localization of labeled cells on MR images [6]. Oligodendroglial progenitors derived from neural stem cells were also magnetically labeled *in vitro* and transplanted intraventricularly in the brain of neonatal rats for a successful *in vivo* MRI tracking [37]. The possibility to repair spinal cord injuries has been investigated also by studying the migration and behavior of transplanted labeled stem cells. Marrow stromal cells (multipotent progenitor cells extracted from bone marrow) were labeled with SPIO (Endorem®) and intravenously injected into rats 1 week after induction of a spinal cord injury. It was observed that the paraplegic rats showed good scores of recovery from the locomotor and the hind limb sensitivity points of view during the 5 weeks following marrow stromal cell injection. Hypointense areas observed in *ex vivo* MRI suggested a migration of the SPIO-labeled cells to the lesion site, and histology confirmed the presence of iron-loaded cells in the lesion. Furthermore, a reduction of the lesion size was noticed in marrow stromal cell-injected animals, suggesting tissue regeneration due to these cells. As the regeneration of axons can be affected by the formation of scar tissue in the injured region, biocompatible macroporous hydrogels (pore size: 10–50 μm) have been used to anatomically replace a removed part of the spinal cord and prevent scarring. A block of hydrogel seeded with SPIO-labeled marrow stromal cells was inserted in the place of the right half of a spinal cord segment and was visible by MRI. Hydrogels create an environment where intrinsic growth factors can diffuse and promote marrow stromal cell migration. Indeed, 6 weeks after implantation, the hydrogel was adherent to the spinal segments and neurofilaments were stained inside by immunohistochemistry, demonstrating the growth of axons into the hydrogel [28]. Another central nervous system injury requiring a replacement of lost cells is cerebral stroke. In the context of brain lesions, the fate (migration and differentiation) of *in vivo* implanted stem cells, after magnetic labeling in culture, has been monitored by the noninvasive MRI technique. The behavior of marrow stromal cells, embryonic stem cells (ESCs), and $CD34^+$ hematopoietic progenitor cells in the injured brain has been studied using a model of cortical photochemical lesion. On T2-weighted MR images, SPIO-labeled marrow stromal cells were visible as a hypointense signal at the level of their implantation site, in the hemisphere contralateral to the lesion. A signal darkening was noticed within 1 and 3 weeks in the damaged cortical tissue, around the necrotic part of the lesion, suggesting a migration of labeled cells. Immunohistochemistry revealed that a small proportion (less than 3%) of the large population of iron-loaded cells present in the lesion expressed the neuronal marker NeuN. Intravenously injected SPIO-labeled marrow stromal cells infiltrated the damaged hemisphere at the border of the lesion. The presence of labeled cells was visible by MRI

and confirmed by histology [26, 28]. The same type of experiment was performed with ESCs. However, to avoid the risk of forming embryonic tumors once grafted *in vivo*, ESCs were differentiated into neural stem cells before implantation. These ESCs were SPIO-labeled and intravenously or intracerebrally (contralateral to the lesion) injected into rats 1 week after the induction of a photochemical cortical lesion. In both cases, MRI revealed a hypointense signal in the lesion 1–2 weeks after injection or implantation. As ESCs were modified to express a fluorescent marker (green fluorescent protein, GFP), fluorescence microscopy performed on histological slices confirmed the presence of labeled cells in this injured site. MRI and histology results also suggested that intracerebrally implanted cells were migrating across the corpus callosum to reach the lesion. Iron-loaded ESCs found in the injured region after intravenous injection were observed to achieve a final differentiation and were identified as mostly astrocytes (70%), but also oligodendrocytes (1%) and neurons (5%) [27, 28]. Under the same experimental conditions, magnetically labeled human $CD34^+$ cells were observed to reach the lesioned target 24 h after contralateral implantation [28]. In other studies, ESCs magnetically labeled with USPIO (Sinerem®) combined to lipofection agent have been implanted in the brain of rats suffering from a focal cerebral ischemia. Two weeks after this induced stroke, labeled cells were implanted in the contralateral hemisphere and observed by MRI. A line of hypointense signal was visualized along the corpus callosum 6 days after grafting of the cells, suggesting a migration of the cells toward the lesion. Indeed, 2 days later, the ischemic hemisphere became darker, suggesting that labeled cells had moved from the injection site and accumulated in the damaged area. Once again, other techniques, such as immunocytochemistry, confirmed the presence of implanted cells in the areas of MR signal darkening. Furthermore, changes in the labeled cells' shape suggested that their differentiation occurred during their migration. Neuron-like cells were observed in the ischemic area [42]. This phenomenon of transplanted stem cells attracted by an ischemic site in the brain has also been observed with neural stem cells labeled using a bimodal contrast agent, the GRID, which allowed for the detection of cells by MRI and fluorescent microscopy [78]. The migration of iron oxide-labeled marrow stromal cells and neural progenitor cells toward another type of brain injury, a gliosarcoma, also has been observed by MRI after the injection of cells in a tail vein or in a subarachnoid space: the cisterna magna [79]. Stem cell transplantation can also be important as a therapy for neurodegenerative diseases. GRID-labeled neural stem cells were intracerebrally transplanted in a rat model of Huntington disease and observed to infiltrate the damaged hemisphere, migrating from their contralateral transplantation site [3].

Another possibility to track magnetically labeled stem cells in the context of ischemic injury has been tested in a model of swine myocardial infarction. Mesenchymal stem cells labeled with fluorescent micrometer-sized particles of iron oxide (MPIO) were percutaneously injected into the intact or infarcted myocardium. Signal darkening was detected in the beating normal or infarcted heart using cardiac MRI (fast gradient echo (FGE) or steady-state free precession (SSFP)) until 3 weeks after the cells' implantation (confirmed *ex vivo* by MRI and histology). Fluorescence microscopy performed on histological slices showed that implanted mesenchymal stem cells were elongated and aligned with the host myocardium, suggesting their *in vivo* differentiation [80]. Using a similar model, SPIO-labeled mesenchymal stem cells were injected in the infarct and could be visualized by *in vivo* MRI until 1 week postimplantation. However, MRI also suggested that the size of the lesion increased and that the negative contrast decreased. Possible explanations for the loss of contrast were division of mesenchymal stem cells inducing a SPIO dilution, a migration of labeled cells, or eventually both [81]. In the same myocardial infarction

model, SPIO-labeled myogenic precursor cells were injected in the infarcted area of pig's heart. The necrotic region was identified in the left ventricle through endoventricular electromechanical mapping, as the part of the myocardium with the most reduced electrical and mechanical activity. Implantation sites of labeled myogenic precursor cells were detected *in vivo* by cardiac MRI and *ex vivo* by iron staining on histological slices [82]. Other experiments have been performed in rats or mice. Rat smooth muscle cells labeled with dimercaptosuccinic acid-coated particles (anionic particles) were implanted in rat hearts with ischemic injury. MR imaging of implantation sites was performed *ex vivo* on the heart excised from 2 to 48 h after grafting of cells. An anatomical correlation between the hypointense signal in myocardium (in T2- or $T2^*$-weighted MRI) and the labeled cells detected in histology or immunohistochemistry was observed [83]. SPIO-labeled ESCs have also been visualized *in vivo* by T2-weighted MRI of the left ventricle of the intact rat heart [84]. Magnetically labeled cardiac progenitor cells have been transplanted into the healthy or injured myocardium of mice. High-resolution MRI allowed the precise determination of the location of labeled cells in the mouse's heart. It was observed that a cardiac ischemic lesion appeared as a hyposignal area, similarly sized on both $T2^*$-weighted and proton density-weighted MR images. However, after transplantation of iron oxide-loaded cardiac progenitor cells to the infarcted mouse myocardium, the signal attenuation area noticed on proton density MR images reflected only the lesion size, while it was larger on $T2^*$-weighted MR images because of the higher detection sensitivity of magnetically labeled cells allowed by the latter parameter weighting [85].

In order to target other potentially damaged organs with stem cells, the fate of SPIO-labeled mesenchymal stem cells injected into the portal veins of rats treated with carbon tetrachloride to induce centrolobular liver necrosis, as well as into the renal arteries of healthy rats, has been studied by MRI and correlated to the histological observation of the iron-loaded cells' distribution in the liver or kidney [86]. However, further experiments have shown that SPIO-labeled mesenchymal stem cells systemically injected (i.e., intravenously and not through the feeding artery) in rats with kidney mesangiolysis homed to the injured kidney but were below the *in vivo* MRI detection threshold. Only *ex vivo* images of the kidneys showed areas of lower intensity that were correlated to iron staining by histology [87].

Type 1 diabetes mellitus has been treated experimentally with another kind of cell therapy. Instead of stem cells, pancreatic islets containing β-cells (producing insulin) were transplanted into the liver of diabetic rats through injection in the portal vein. The pancreatic islets were magnetically labeled with SPIO (Resovist®) and their hepatic location was visualized by MRI. The labeled pancreatic islets, situated in the liver sinusoids, were observed as hypointense areas homogeneously distributed in the liver. Furthermore, a normal glycemia was restored in previously diabetic rats 1 week after transplantation of the islets [88].

14.6.2 MRI Monitoring of Cells After Magnetic Labeling *In Vivo*

Visualizing cells *in vivo* by MRI without any *in vitro* magnetic prelabeling requires a sufficient cellular uptake of the MRI contrast agent provided by the blood circulation after intravenous administration.

Inflammation Hepatic MRI using iron oxides is based on the capture of nanoparticles by the resident macrophages of the liver: the Kupffer cells. As inflammatory diseases are associated with monocyte/macrophage activity, this macrophage targeting approach has been

further developed to visualize inflammatory lesions in the body. Thus following intravenous injection of iron oxide nanoparticles, inflammatory foci can be visualized by MRI. This has been achieved in experimental models of brain inflammatory diseases. After administration of USPIO (Sinerem®) at a concentration of 300 μmol Fe/kg, macrophage activity was imaged in rats with experimental autoimmune encephalomyelitis (EAE), thanks to the capture of the nanoparticles by peripheral macrophages (blood monocytes or lymph node macrophages) subsequently invading the inflamed brain. However, the injected iron dose was about seven times higher than the appropriate dose for human use (45 μmol Fe/kg (2.6 mg/kg)). This was explained by the fact that a high iron dose is necessary to saturate the uptake capability of liver, spleen, or bone marrow macrophages. Furthermore, at the normal dose, the blood half-life of Sinerem® in rats is only 2 h, while it is 20–24 h in humans [89]. In rat models of cerebral stroke, infiltration of macrophages in ischemic lesions has also been visualized by MRI following USPIO uptake. The localization of these hypointense areas on T2-weighted MR images was correlated to the histological detection of iron and to the immunohistological labeling of macrophages postmortem [90, 91]. In this context of brain damages associated with inflammatory events, macrophage activity has been studied by MRI after USPIO infusion also in human patients suffering from stroke [92]. *In vivo* cellular MR imaging of USPIO-labeled macrophages has found successful applications in other animal models of disease, such as in kidney injuries (nephropathies) induced by a nephrotoxic drug (puromycin aminonucleoside) or in organ graft rejection (e.g., after renal allograft transplantation without any immunosuppressive drug) [3, 93, 94]. The accumulation of long-circulating USPIO in monocytes and macrophages recruited to atherosclerotic plaques has been demonstrated also in hyperlipidemic rabbits [95, 96]. Furthermore, USPIO-enhanced MRI has also been used for *in vivo* detection of macrophages in human plaques. The strongest signal decreases, due to iron-loaded macrophage accumulation, were observed in ruptured and rupture-prone human atherosclerotic lesions rather than in stable lesions, allowing for a differentiation between low-risk and high-risk plaques on MR images [3, 97]. MPIO also have been intravenously injected into rats with the aim of labeling macrophage infiltrates in the rejection site of cardiac graft, allowing for the noninvasive monitoring of organ transplant rejection by MRI [98].

Tumors The *in vivo* tumoral accumulation of iron oxide nanoparticles has been investigated given the great interest of detecting tumors by MRI. In a rat model of intracerebrally implanted glioma, MION were intravenously injected (10 mg Fe/kg) and induced a signal increase of the tumor on T1-weighted MR images and a signal decrease on T2-weighted MR images, particularly at the tumoral periphery, 24 h after injection. Microscopic and histological examinations showed that the nanoparticles were intracellularly and extracellularly distributed in the tumor, with a higher level of accumulation in the periphery. Indeed, the highest microvascular density of a tumor is found in this area, which is consequently a region of preferential extravasation. Tumor-associated macrophages and vascular endothelial cells were observed to take up the nanoparticles, but the majority of nanoparticle-containing cells were tumor cells. Furthermore, the cellular uptake of the nanoparticles seems to be directly related to the tumor growth—in other words, directly related to the cellular cycle [19]. The same type of MION distribution in the tumor cells adjacent to the hyperpermeable tumor–brain interface has been reported in another study [99]. USPIO were injected intravenously into rats bearing intracerebral tumors (LX-1 small-cell lung carcinoma) and did not show the same distribution pattern as MION. Within 24 h postinjection, T1-weighted MR images showed an enhancement of the signal at the periphery of the tumor, surrounding a

brighter region corresponding to a necrotic core. Histological analysis allowed for the detection of iron in and around necrotic areas, and at the tumor margin, but only in macrophages, reactive astrocytes, or gliosis (scar made of a dense fibrous network of neuroglia). Regarding LX-1 small-cell lung carcinoma, other tumor types exhibited a weaker T1-enhancement pattern with USPIO and consequently showed a sparser iron staining in histology, but confirmed the distribution of the nanoparticles in cells infiltrated at the brain–tumor interface and in areas of necrosis. It was noticed that bigger nanoparticles (SPIO, Feridex®), rapidly captured by spleen or liver macrophages, were ineffective for imaging brain tumors [100]. MION and USPIO are long-circulating iron oxide nanoparticles, able to passively target tumors by extravasation through the leaky tumoral capillaries. This interstitial accumulation of USPIO has also been suggested by a tumoral signal enhancement in T1-weighted MRI, 12 h after intravenous injection of the nanoparticles in mice bearing nonnecrotic subcutaneously implanted tumors (human prostatic adenocarcinoma). However, a signal decrease of the tumor was generated in T2-weighted MRI by dimercaptosuccinic acid-coated anionic iron oxide nanoparticles, 24 h postinjection. It suggested an intracellular tumoral distribution of these nanoparticles [101]. Magnetic labeling of tumors has also been achieved by magnetically targeting liposomes loaded with iron oxide nanoparticles to human prostatic adenocarcinoma implanted in mice. A preferential accumulation of these polyethylene glycol-coated long-circulating magnetoliposomes (200 nm in diameter) was induced by placing a magnet on the skin above the tumor during the circulation of the intravenously injected magnetoliposomes. MRI showed a strong signal darkening of the tumor exposed for 24 h to the magnet, compared to nonexposed tumors. It was observed that, due to a higher global magnetic moment, the magnetoliposomes could be magnetically driven to a tumor more efficiently than nonencapsulated USPIO. The mechanism of tumoral accumulation of magnetoliposomes is diffusion to the interstitium, through the leaky vasculature. Histological analysis revealed the presence of magnetoliposomes mainly in the most highly vascularized zones: in capillaries, interstitium, and cells (macrophages, fibroblasts, endothelial cells), but not in tumor cells. Iron was also found in liver and spleen [102]. Paramagnetic contrast agents have also been used as tumor-specific contrast agents *in vivo*. Gd-based metalloporphyrins, such as Gadophrin-2 (Bayer Schering Pharma AG), can selectively accumulate in tumors because of their high affinity to necrotic tissues. It has been suggested that their ability to bind plasma albumin is responsible for their slow extravasation and subsequent accumulation into the necrotic tumor interstitium [103, 104].

14.7 CONCLUSION AND PERSPECTIVES

Iron oxide particles, made of polymer- or monomer-coated iron oxide crystals, are well known in clinical applications as intravenously injected negative MRI contrast agents. *In vivo*, they are sooner (for larger ones) or later (for smaller ones) taken up by cells of the mononuclear phagocyte system. Iron oxide particles have been presented as an interesting tool for cellular magnetic labeling because of their greater effect on the MR signal as compared to paramagnetic ions, allowing their MRI detection at relatively low concentrations (nanomolar) in tissues and thus opening the field of cellular MRI research. The ability of iron oxide particles to be taken up by phagocytic cells after intravenous injection has been further exploited to image macrophage-invaded areas in the context of inflammatory pathologies or tumors. MRI monitoring of nonphagocytic cells is often possible by a magnetic labeling of these cells performed *in vitro*, prior to their *in vivo* implantation. In

other terms, iron oxide particles must be internalized by cultured cells in an optimal way. In many cases, particles are used unmodified (polymer- or monomer-coated iron oxide crystals) or they can be unspecifically cell-targeted (mixed with DNA transfection reagents, conjugated to a cell-penetrating peptide), triggering their endocytosis via nonspecific pathways. Iron oxide nanoparticles can also be linked to a ligand specific for a certain receptor at the cell surface, allowing their receptor-mediated uptake. In brief, the magnetic labeling of cells with MRI contrast agents, in particular, with iron oxide nanoparticles, is receiving increasing attention since *in vivo* applications exist in different pathological contexts. Since they are taken up by phagocytic cells, SPIO (Feridex® (Endorem®), Resovist®) were originally developed and approved for clinical MRI to increase the lesion-to-liver contrast in malignancies where Kupffer cells are absent. It is worth mentioning that these SPIO were recently taken off the market due to lack of sales in that context. Nevertheless, they were used for cellular magnetic labeling studies in patients, suggesting that a great deal of future research and development will be driven in the field of cellular magnetic labeling and cellular MRI [105].

REFERENCES

1. Artemov, D.; Mori, N.; Okollie, B.; Bhujwalla, Z. M. MR molecular imaging of the Her-2/neu receptor in breast cancer cells using targeted iron oxide nanoparticles, *Magn. Reson. Med.* **2003**, *49*, 403–408.
2. Bulte, J. W. M.; Modo, M. M. J. *Nanoparticles in Biomedical Imaging, Emerging Technologies and Applications*. Springer: New York, 2007.
3. Modo, M.; Hoehn, M.; Bulte, J. W. Cellular MR imaging, *Mol. Imaging* **2005**, *4*, 143–164.
4. Hopkins, C. R.; Trowbridge, I. S. Internalization and processing of transferrin and the transferrin receptor in human carcinoma A431 cells. *J. Cell Biol*. **1983**, *97*, 508–521.
5. Kresse, M.; Wagner, S.; Pfefferer, D.; Lawaczeck, R.; Elste, V.; Semmler, W. Targeting of ultrasmall superparamagnetic iron oxide (USPIO) particles to tumor cells in vivo by using transferrin receptor pathways. *Magn. Reson. Med*. **1998**, *40*, 236–242.
6. Bulte, J. W.; Zhang, S.; van Gelderen, P.; Herynek, V.; Jordan, E. K.; Duncan, I. D.; Frank, J. A. Neurotransplantation of magnetically labeled oligodendrocyte progenitors: magnetic resonance tracking of cell migration and myelination. *Proc. Natl. Acad. Sci. U.S.A*. **1999**, *96*, 15256–15261.
7. Weissleder, R.; Moore, A.; Mahmood, U.; Bhorade, R.; Benveniste, H.; Chiocca, E. A.; Basilion, J. P. *In vivo* magnetic resonance imaging of transgene expression. *Nat. Med*. **2000**, *6*, 351–355.
8. Deans, A. E.; Wadghiri, Y. Z.; Bernas, L. M.; Yu, X.; Rutt, B. K.; Turnbull, D. H. Cellular MRI contrast via coexpression of transferrin receptor and ferritin. *Magn. Reson. Med*. **2006**, *56*, 51–59.
9. Harrison, P. M.; Arosio, P. The ferritins: molecular properties, iron storage function and cellular regulation. *Biochim. Biophys. Acta* **1996**, *1275*, 161–203.
10. Treffry, A.; Zhao, Z.; Quail, M. A.; Guest, J. R.; Harrison, P. M. Dinuclear center of ferritin: studies of iron binding and oxidation show differences in the two iron sites. *Biochemistry*. **1997**, *36*, 432–441.
11. Cohen, B.; Dafni, H.; Meir, G.; Harmelin, A.; Neeman, M. Ferritin as an endogenous MRI reporter for noninvasive imaging of gene expression in C6 glioma tumors. *Neoplasia*. **2005**, *7*, 109–117.
12. Wang, Z. J.; Boddington, S.; Wendland, M.; Meier, R.; Corot, C.; Daldrup-Link, H. MR imaging of ovarian tumors using folate-receptor-targeted contrast agents. *Pediatr. Radiol*. **2008**, *38*, 529–537.

13. Sun, C.; Veiseh, O.; Gunn, J.; Fang, C.; Hansen, S.; Lee, D.; Sze, R.; Ellenbogen, R. G.; Olson, J.; Zhang, M. In vivo MRI detection of gliomas by chlorotoxin-conjugated superparamagnetic nanoprobes. *Small* **2008**, *4*, 372–379.
14. Serda, R. E.; Adolphi, N. L.; Bisoffi, M.; Sillerud, L. O. Targeting and cellular trafficking of magnetic nanoparticles for prostate cancer imaging. *Mol. Imaging* **2007**, *6*, 277–288.
15. Yang, L.; Mao, H.; Wang, Y. A.; Cao, Z.; Peng, X.; Wang, X.; Duan, H.; Ni, C.; Yuan, Q.; Adams, G.; Smith, M. Q.; Wood, W. C.; Gao, X.; Nie, S. Single chain epidermal growth factor receptor antibody conjugated nanoparticles for in vivo tumor targeting and imaging. *Small* **2009**, *5*, 235–243.
16. Leuschner, C.; Kumar, C. S.; Hansel, W.; Soboyejo, W.; Zhou, J.; Hormes, J. LHRH-conjugated magnetic iron oxide nanoparticles for detection of breast cancer metastases. *Breast Cancer Res. Treat*. **2006**, *99*, 163–176.
17. Anderson, S. A.; Glod, J.; Arbab, A. S.; Noel, M.; Ashari, P.; Fine, H. A.; Frank, J. A. Noninvasive MR imaging of magnetically labeled stem cells to directly identify neovasculature in a glioma model. *Blood* **2005**, *105*, 420–425.
18. Moore, A.; Weissleder, R.; Bogdanov, A. Uptake of dextran-coated monocrystalline iron oxides in tumor cells and macrophages. *J. Magn. Reson. Imaging* **1997**, *7*, 1140–1145.
19. Moore, A.; Marecos, E.; Bogdanov, A.; Weissleder, R. Tumoral distribution of long-circulating dextran-coated iron oxide nanoparticles in a rodent model. *Radiology* **2000**, *214*, 568–574.
20. Modo, M.; Cash, D.; Mellodew, K.; Williams, S. C.; Fraser, S. E.; Meade, T. J.; Price, J.; Hodges, H. Tracking transplanted stem cell migration using bifunctional, contrast agent-enhanced, magnetic resonance imaging. *Neuroimage* **2002**, *17*, 803–811.
21. Crich, S. G.; Biancone, L.; Cantaluppi, V.; Duo, D.; Esposito, G.; Russo, S.; Camussi, G.; Aimé, S. Improved route for the visualization of stem cells labeled with a Gd-/Eu-chelate as dual (MRI and fluorescence) agent. *Magn. Reson. Med. Engl*. **2004**, *51*, 938–944.
22. Aimé, S.; Carrera, C.; Delli Castelli, D.; Crich, S. G.; Terreno, E. Tunable imaging of cells labeled with MRI-PARACEST agents. *Angew. Chem. Int. Ed*. **2005**, *44*, 1813–1815.
23. Rudelius, M.; Daldrup-Link, H. E.; Heinzmann, U.; Piontek, G.; Settles, M.; Link, T. M.; Schlegel, J. Highly efficient paramagnetic labelling of embryonic and neuronal stem cells. *Eur. J. Nucl. Med. Mol. Imaging* **2003**, *30*, 1038–1044.
24. Schoepf, U.; Mercos, E. M.; Melder, R. J.; Jain, R. K.; Weissleder, R. Intracellular magnetic labeling of lymphocytes for *in vivo* trafficking studies. *Biotechniques* **1998**, *24*, 642–646, 648–651.
25. Yeh, T. C.; Zhang, W.; Ildstad, S. T.; Ho, C. Intracellular labeling of T-cells with superparamagnetic contrast agents. *Magn. Reson. Med*. **1993**, *30*, 617–625.
26. Jendelova, P.; Herynek, V.; DeCroos, J.; Glogarova, K.; Andersson, B.; Hajek, M.; Sykova, E. Imaging the fate of implanted bone marrow stromal cells labeled with superparamagnetic nanoparticles. *Magn. Reson. Med*. **2003**, *50*, 767–776.
27. Jendelova, P.; Herynek, V.; Urdzikova, L.; Glogarova, K.; Kroupova, J.; Andersson, B.; Bryja, V.; Burian, M.; Hajek, M.; Sykova, E. Magnetic resonance tracking of transplanted bone marrow and embryonic stem cells labeled by iron oxide nanoparticles in rat brain and spinal cord. *J. Neurosci. Res*. **2004**, *76*, 232–243.
28. Sykova, E.; Jendelova, P. Magnetic resonance tracking of implanted adult and embryonic stem cells in injured brain and spinal cord. *Ann. N.Y. Acad. Sci.*. **2005**, *1049*, 146–160.
29. Daldrup-Link, H. E.; Rudelius, M.; Oostendorp, R. A.; Settles, M.; Piontek, G.; Metz, S.; Rosenbrock, H.; Keller, U.; Heinzmann, U.; Rummeny, E. J.; Schlegel, J.; Link, T. M. Targeting of hematopoietic progenitor cells with MR contrast agents. *Radiology* **2003**, *228*, 760–767.
30. Mailänder, V.; Lorenz, M. R.; Holzapfel, V.; Musyanovych, A.; Fuchs, K.; Wiesneth, M.; Walther, P.; Landfester, K.; Schrezenmeier, H. Carboxylated superparamagnetic iron oxide

particles label cells intracellularly without transfection agents. *Mol. Imaging Biol*. **2008**, *10*, 138–146.

31. Kalish, H.; Arbab, A. S.; Miller, B. R.; Lewis, B. K.; Zywicke, H. A.; Bulte, J. W.; Bryant, L. H., Jr; Frank, J. A. Combination of transfection agents and magnetic resonance contrast agents for cellular imaging: relationship between relaxivities, electrostatic forces, and chemical composition. *Magn. Reson. Med.* **2003**, *50*, 275–282.
32. Bulte, J. W. Magnetic nanoparticles as markers for cellular MR imaging. *J. Magn. Magn. Mater*. **2005**, *289*, 423–427.
33. Frank, J. A.; Miller, B. R.; Arbab, A. S.; Zywicke, H. A.; Jordan, E. K.; Lewis, B. K.; Bryant, L. H.; Bulte, J. W. Clinically applicable labeling of mammalian and stem cells by combining superparamagnetic iron oxides and transfection agents. *Radiology* **2003**, *228*, 480–487.
34. Arbab, A. S.; Yocum, G. T.; Wilson, L. B.; Parwana, A.; Jordan, E. K.; Kalish, H.; Frank, J. A. Comparison of transfection agents in forming complexes with ferumoxides, cell labeling efficiency, and cellular viability. *Mol. Imaging* **2004**, *3*, 24–32.
35. Arbab, A. S.; Yocum, G. T.; Kalish, H.; Jordan, E. K.; Anderson, S. A.; Khakoo, A. Y.; Read, E. J.; Frank, J. A. Efficient magnetic cell labeling with protamine sulfate complexed to ferumoxides for cellular MRI. *Blood* **2004**, *104*, 1217–1223.
36. *Superfect® Transfection Reagent Handbook, For High Transfection Efficiencies in a Broad Range of Cell Lines*. Qiagen Valencia, CA, 2000.
37. Bulte, J. W.; Douglas, T.; Witwer, B.; Zhang, S. C.; Strable, E.; Lewis, B. K.; Zywicke, H.; Miller, B.; van Gelderen, P.; Moskowitz, B. M.; Duncan, I. D.; Frank, J. A. Magnetodendrimers allow endosomal magnetic labeling and *in vivo* tracking of stem cells. *Nat. Biotechnol*. **2001**, *19*, 1141–1147.
38. Klajnert, B.; Bryszewska, M. Dendrimers: properties and applications. *Acta. Biochim. Pol*. **2001**, *48*, 199–208.
39. Wilhelm, C.; Billotey, C.; Roger, J.; Pons, J. N.; Bacri, J. C.; Gazeau, F. Intracellular uptake of anionic superparamagnetic nanoparticles as a function of their surface coating. *Biomaterials* **2003**, *24*, 1001–1011.
40. Boutry, S.; Brunin, S.; Mahieu, I.; Laurent, S.; Vander Elst, L.; Muller, R. N. Magnetic labeling of non-phagocytic adherent cells with iron oxide nanoparticles: a comprehensive study. *Contrast Media Mol. Imaging* **2008**, *3*, 223–232.
41. Wrobel, I.; Collins, D. Fusion of cationic liposomes with mammalian cells occurs after endocytosis. *Biochim. Biophys. Acta* **1995**, *1235*, 296–304.
42. Hoehn, M.; Kustermann, E.; Blunk, J.; Wiedermann, D.; Trapp, T.; Wecker, S.; Focking, M.; Arnold, H.; Hescheler, J.; Fleischmann, B. K.; Schwindt, W.; Buhrle, C. Monitoring of implanted stem cell migration *in vivo:* a highly resolved in vivo magnetic resonance imaging investigation of experimental stroke in rat. *Proc. Natl. Acad. Sci. U.S.A*. **2002**, *99*, 16267–16272.
43. van den Bos, E. J.; Wagner, A.; Mahrholdt, H.; Thompson, R. B.; Morimoto, Y.; Sutton, B. S.; Judd, R. M.; Taylor, D. A. Improved efficacy of stem cell labeling for magnetic resonance imaging studies by the use of cationic liposomes. *Cell Transplant*. **2003**, *12*, 743–756.
44. Vives, E.; Brodin, P.; Lebleu, B. A truncated HIV-1 Tat protein basic domain rapidly translocates through the plasma membrane and accumulates in the cell nucleus. *J. Biol. Chem*. **1997**, *272*, 16010–16017.
45. Potocky, T. B.; Menon, A. K.; Gellman, S. H. Cytoplasmic and nuclear delivery of a TAT-derived peptide and a beta-peptide after endocytic uptake into HeLa cells. *J. Biol. Chem*. **2003**, *278*, 50188–50194.
46. Vives, E.; Richard, J. P.; Rispal, G.; Lebleu, B. TAT peptide internalization: seeking the mechanism of entry. *Curr. Protein. Pept. Sci*. **2003**, *4*, 125–132.

47. Iozzo, R. V. Heparan sulfate proteoglycans: intricate molecules with intriguing functions. *J. Clin. Invest*. **2001**,*108*, 165–167.

48. Bhorade, R.; Weissleder, R.; Nakakoshi, T.; Moore, A.; Tung, C. H. Macrocyclic chelators with paramagnetic cations are internalized into mammalian cells via a HIV-tat derived membrane translocation peptide. *Bioconjug. Chem*. **2000**, *11*, 301–305.

49. Prantner, A. M.; Sharma, V.; Garbow, J. R.; Piwnica-Worms, D. Synthesis and characterization of a Gd-DOTA-D-permeation peptide for magnetic resonance relaxation enhancement of intracellular targets. *Mol. Imaging* **2003**, *2*, 333–341.

50. Lewin, M.; Carlesso, N.; Tung, C. H.; Tang, X. W.; Cory, D.; Scadden, D. T.; Weissleder, R. Tat peptide-derivatized magnetic nanoparticles allow *in vivo* tracking and recovery of progenitor cells. *Nat. Biotechnol*. **2000**, *18*, 410–414.

51. Josephson, L.; Tung, C. H.; Moore, A.; Weissleder, R. High-efficiency intracellular magnetic labeling with novel superparamagnetic-Tat peptide conjugates. *Bioconjug. Chem*. **1999**, *10*, 186–191.

52. Tung, C. H.; Weissleder, R. Arginine containing peptides as delivery vectors. *Adv. Drug. Deliv. Rev*. **2003**, *55*, 281–294.

53. Walczak, P.; Kedziorek, D. A.; Gilad, A. A.; Lin, S.; Bulte, J. W. Instant MR labeling of stem cells using magnetoelectroporation. *Magn. Reson. Med*. **2005**, *54*, 769–774.

54. Hinds, K. A.; Hill, J. M.; Shapiro, E. M.; Laukkanen, M. O.; Silva, A. C.; Combs, C. A.; Varnet, T. R.; Balaban, R. S.; Koretsky, A. P.; Dunbar, C. E. Highly efficient endosomal labeling of progenitor and stem cells with large magnetic particles allows magnetic resonance imaging of single cells. *Blood* **2003**, *102*, 867–872.

55. Shapiro, E. M.; Skrtic, S.; Koretsky, A. P. Sizing it up: cellular MRI using micron-sized iron oxide particles. *Magn. Reson. Med*. **2005**, *53*, 329–338.

56. Weisskoff, R. M.; Zuo, C. S.; Boxerman, J. L.; Rosen, B. R. Microscopic susceptibility variation and transverse relaxation: theory and experiment. *Magn. Reson. Med*. **1994**, *31*, 601–610.

57. Shapiro, E. M.; Skrtic, S.; Sharer, K.; Hill, J. M.; Dunbar, C. E.; Koretsky, A. P. MRI detection of single particles for cellular imaging. *Proc. Natl. Acad. Sci. U.S.A*. **2004**, *101*, 10901–10906.

58. Shapiro, E. M.; Sharer, K.; Skrtic, S.; Koretsky, A. P. *In vivo* detection of single cells by MRI. *Magn. Reson. Med*. **2006**, *55*, 242–249.

59. Raynal, I.; Prigent, P.; Peyramaure, S.; Najid, A.; Rebuzzi, C.; Corot, C. Macrophage endocytosis of superparamagnetic iron oxide nanoparticles: mechanisms and comparison of ferumoxides and ferumoxtran-10. *Invest. Radiol*. **2004**, *39*, 56–63.

60. Palecanda, A.; Paulauskis, J.; Al-Mutairi, E.; Imrich, A.; Qin, G.; Suzuki, H.; Kodama, T.; Tryggvason, K.; Koziel, H.; Kobzik, L. Role of the scavenger receptor MARCO in alveolar macrophage binding of unopsonized environmental particles. *J. Exp. Med*. **1999**, *189*, 1497–1506.

61. Fleige, G.; Seeberger, F.; Laux, D.; Kresse, M.; Taupitz, M.; Pilgrimm, H.; Zimmer, C. *In vitro* characterization of two different ultrasmall iron oxide particles for magnetic resonance cell tracking. *Invest. Radiol*. **2002**, *37*, 482–488.

62. Champion, J. A.; Mitragotri, S. Role of target geometry in phagocytosis. *Proc. Natl. Acad. Sci. U.S.A*. **2006**, *103*, 4930–4934.

63. Jelezarova, E.; Luginbuehl, A.; Lutz, H. U. C3b2-IgG complexes retain dimeric C3 fragments at all levels of inactivation. *J. Biol. Chem*. **2003**, *278*, 51806–51812.

64. Ahrens, E. T.; Feili-Hariri, M.; Xu, H.; Genove, G.; Morel, P. A. Receptor-mediated endocytosis of iron-oxide particles provides efficient labeling of dendritic cells for *in vivo* MR imaging. *Magn. Reson. Med*. **2003**, *49*, 1006–1013.

65. Himmelreich, U.; Aimé, S.; Hyeronymus, T.; Justicia, C.; Uggeri, F.; Zenke, M.; Hoehn, M. A responsive MRI contrast agent to monitor functional cell status. *Neuroimage* **2006**, *32*, 1142–1149.

66. Kostura, L.; Kraitchman, D. L.; Mackay, A. M.; Pittenger, M. F.; Bulte, J. W. Feridex labeling of mesenchymal stem cells inhibits chondrogenesis but not adipogenesis or osteogenesis. *NMR Biomed*. **2004**, *17*, 513–517.

67. Arbab, A. S.; Bashaw, L. A.; Miller, B. R.; Jordan, E. K.; Bulte, J. W.; Frank, J. A. Intracytoplasmic tagging of cells with ferumoxides and transfection agent for cellular magnetic resonance imaging after cell transplantation: methods and techniques. *Transplantation* **2003**, *76*, 1123–1130.

68. Stroh, A.; Zimmer, C.; Gutzeit, C.; Jackstadt, M.; Marschinke, F.; Jung, T.; Pilgrimm, H.; Grune, T. Iron oxide particles for molecular magnetic resonance imaging cause transient oxidative stress in rat macrophages. *Free Radic. Biol. Med*. **2004**, *36*, 976–984.

69. Neri, M.; Maderna, C.; Cavazzin, C.; Deidda-Vigoriti, V.; Politi, L. S.; Scotti, G.; Marzola, P.; Sbarbati, A.; Vescovi, A.L.; Gritti, A. Efficient in vitro labeling of human neural precursor cells with superparamagnetic iron oxide particles: relevance for in vivo cell tracking. *Stem. Cells* **2008**, *26*, 505–516.

70. Küstermann, E.; Himmelreich, U.; Kandal, K.; Geelen, T.; Ketkar, A.; Wiedermann, D.; Strecker, C.; Esser, J.; Arnhold, S.; Hoehn, M. Efficient stem cell labeling for MRI studies. *Contrast Media Mol. Imaging* **2008**, *3*, 27–37.

71. Smirnov, P.; Gazeau, F.; Lewin, M.; Bacri, J. C.; Siauve, N.; Vayssettes, C.; Cuenod, C. A.; Clement, O. In vivo cellular imaging of magnetically labeled hybridomas in the spleen with a 1.5-T clinical MRI system. *Magn. Reson. Med*. **2004**, *52*, 73–79.

72. Daldrup-Link, H. E.; Rudelius, M.; Piontek, G.; Metz, S.; Brauer, R.; Debus, G.; Corot, C.; Schlegel, J.; Link, T. M.; Peschel, C.; Rummeny, E. J.; Oostendorp, R. A. Migration of iron oxide-labeled human hematopoietic progenitor cells in a mouse model: in vivo monitoring with 1.5-T MR imaging equipment. *Radiology* **2005**, *234*, 197–205.

73. Anderson, S. A.; Shukaliak-Quandt, J.; Jordan, E. K.; Arbab, A. S.; Martin, R.; McFarland, H.; Frank, J. A. Magnetic resonance imaging of labeled T-cells in a mouse model of multiple sclerosis. *Ann. Neurol*. **2004**, *55*, 654–659.

74. Kircher, M. F.; Allport, J. R.; Graves, E. E.; Love, V.; Josephson, L.; Lichtman, A. H.; Weissleder, R. *In vivo* high resolution three-dimensional imaging of antigen-specific cytotoxic T-lymphocyte trafficking to tumors. *Cancer Res*. **2003**, *63*, 6838–6846.

75. Smirnov, P.; Lavergne, E.; Gazeau, F.; Lewin, M.; Boissonnas, A.; Doan, B. T.; Gillet, B.; Combardière, C.; Clément, O. *In vivo* cellular imaging of lymphocyte trafficking by MRI: a tumor model approach to cell-based anticancer therapy. *Magn. Reson. Med*. **2006**, *56*, 498–508.

76. Daldrup-Link, H. E.; Meier, R.; Rudelius, M.; Piontek, G.; Piert, M.; Metz, S.; Settles, M.; Uherek, C.; Wels, W.; Schlegel, J.; Rummeny, E. J. *In vivo* tracking of genetically engineered, anti-HER2/neu directed natural killer cells to HER2/neu positive mammary tumors with magnetic resonance imaging. *Eur. Radiol*. **2005**, *15*, 4–13.

77. de Vries, I. J.; Lesterhuis, W. J.; Barentsz, J. O.; Verdijk, P.; van Krieken, J. H.; Boerman, O. C.; Oyen, W. J.; Bonenkamp, J. J.; Boezeman, J. B.; Adema, G. J.; Bulte, J.W.; Scheenen, T. W.; Punt, C. J.; Heerschap, A.; Figdor, C. G. Magnetic resonance tracking of dendritic cells in melanoma patients for monitoring of cellular therapy. *Nat. Biotechnol*. **2005**, *23*, 1407–1413.

78. Modo, M.; Mellowdew, K.; Cash, D.; Fraser, S. E.; Meade, T. J.; Price, J.; Williams, S. C. Mapping transplanted stem cell migration after a stroke: a serial, in vivo magnetic resonance imaging study. *Neuroimage* **2004**, *21*, 311–317.

79. Zhang, Z.; Jiang, Q.; Jiang, F.; Ding, G.; Zhang, R.; Wang, L.; Zhang, L.; Robin, A. M.; Katakowski, M.; Chopp, M. *In vivo* magnetic resonance imaging tracks adult neural progenitor cell targeting of brain tumor. *Neuroimage* **2004**, *23*, 281–287.

80. Hill, J. M.; Dick, A. J.; Raman, V. K.; Thompson, R. B.; Yu, Z. X.; Hinds, K. A.; Pessanha, B. S.; Guttman, M. A.; Varney, T. R.; Martin, B. J.; Dunbar, C. E.; McVeigh, E. R.; Lederman, R. J. Serial cardiac magnetic resonance imaging of injected mesenchymal stem cells. *Circulation* **2003**, *108*, 1009–1014.

81. Kraitchman, D. L.; Heldman, A. W.; Atalar, E.; Amado, L. C.; Martin, B. J.; Pittenger, M. F.; Hare, J. M.; Bulte, J. W. In vivo magnetic resonance imaging of mesenchymal stem cells in myocardial infarction. *Circulation* **2003**, *107*, 2290–2293.

82. Garot, J.; Unterseeh, T.; Teiger, E.; Champagne, S.; Chazaud, B.; Gherardi, R.; Hittinger, L.; Gueret, P.; Rahmouni, A. Magnetic resonance imaging of targeted catheter-based implantation of myogenic precursor cells into infarcted left ventricular myocardium. *J. Am. Coll. Cardiol.* **2003**, *41*, 1841–1846.

83. Rivière, C.; Boudghene, F. P.; Gazeau, F.; Roger, J.; Pons, J. N.; Laissy, J. P.; Allaire, E.; Michel, J. B.; Letourneur, D.; Deux, J. F. Iron oxide nanoparticle-labeled rat smooth muscle cells: cardiac MR imaging for cell graft monitoring and quantitation. *Radiology* **2005**, *235*, 959–967.

84. Tallheden, T.; Nanmark, U.; Lorentzon, M.; Rakotonirainy, O.; Soussi, B.; Waagstein, F.; Jeppsson, A.; Sjogren-Jansson, E.; Lindhal, A.; Omerovic, E. *In vivo* MR imaging of magnetically labeled human embryonic stem cells. *Life Sci*. **2006**, *79*, 999–1006.

85. Kustermann, E.; Roell, W.; Breitbach, M.; Wecker, S.; Wiedermann, D.; Buehrlr, C.; Welz, A.; Hescheler, J.; Fleischmann, B. K.; Hoehn, M. Stem cell implantation in ischemic mouse heart: a high-resolution magnetic resonance imaging investigation. *NMR Biomed*. **2005**, *18*, 362–370.

86. Bos, C.; Delmas, Y.; Desmouliere, A.; Solanilla, A.; Hauger, O.; Grosset, C.; Dubus, I.; Ivanovic, Z.; Rosenbaum, J.; Charbord, P.; Combe, C.; Bulte, J. W.; Moonen, C. T.; Ripoche, J.; Grenier, N. *In vivo* MR imaging of intravascularly injected magnetically labeled mesenchymal stem cells in rat kidney and liver. *Radiology* **2004**, *233*, 781–789.

87. Hauger, O.; Frost, E. E.; van Heeswijk, R.; Deminiere, C.; Xue, R.; Delmas, Y.; Combe, C.; Moonen, C. T.; Grenier, N.; Bulte, J. W. MR evaluation of the glomerular homing of magnetically labeled mesenchymal stem cells in a rat model of nephropathy. *Radiology* **2006**, *238*, 200–210.

88. Jirak, D.; Kriz, J.; Herynek, V.; Andersson, B.; Girman, P.; Burian, M.; Saudek, F.; Hajek, M. MRI of transplanted pancreatic islets. *Magn. Reson. Med.* **2004**, *52*, 1228–1233.

89. Dousset, V.; Doche, B.; Petry, K. G.; Brochet, B.; Delalande, C.; Caille, J. M. Correlation between clinical status and macrophage activity imaging in the central nervous system of rats. *Acad. Radiol*. **2002**, *9* (Suppl 1), S156–S159.

90. Rausch, M.; Sauter, A.; Frohlich, J.; Neubacher, U.; Radu, E. W.; Rudin, M. Dynamic patterns of USPIO enhancement can be observed in macrophages after ischemic brain damage. *Magn. Reson. Med*. **2001**, *46*, 1018–1022.

91. Schroeter, M.; Saleh, A.; Wiedermann, D.; Hoehn, M.; Jander, S. Histochemical detection of ultrasmall superparamagnetic iron oxide (USPIO) contrast medium uptake in experimental brain ischemia. *Magn. Reson. Med*. **2004**, *52*, 403–406.

92. Saleh, A.; Schroeter, M.; Jonkmanns, C.; Hartung, H. P.; Modder, U.; Jander, S. *In vivo* MRI of brain inflammation in human ischaemic stroke. *Brain* **2004**, *127*, 1670–1677.

93. Hauger, O.; Delalande, C.; Trillaud, H.; Deminiere, C.; Quesson, B.; Kahn, H.; Cambar, J.; Combe, C.; Grenier, N. MR imaging of intrarenal macrophage infiltration in an experimental model of nephrotic syndrome. *Magn. Reson. Med.* **1999**, *41*, 156–162.

94. Beckmann, N.; Cannet, C.; Fringeli-Tanner, M.; Baumann, D.; Pally, C.; Bruns, C.; Zerwes, H. G.; Andriambeloson, E.; Bigaud, M. Macrophage labeling by SPIO as an early marker of

allograft chronic rejection in a rat model of kidney transplantation. *Magn. Reson. Med.* **2003**, *49*, 459–467.

95. Weinmann, H. J.; Ebert, W.; Misselwitz, B.; Schmitt-Willich, H. Tissue-specific MR contrast agents. *Eur. J. Radiol*. **2003**, *46*, 33–44.
96. Ruehm, S. G.; Corot, C.; Vogt, P.; Kolb, S.; Debatin, J. F. Magnetic resonance imaging of atherosclerotic plaque with ultrasmall superparamagnetic particles of iron oxide in hyperlipidemic rabbits. *Circulation* **2001**, *103*, 415–422.
97. Kooi, M. E.; Cappendijk, V. C.; Cleutjens, K. B.; Kessels, A. G.; Kitslaar, P. J.; Borgers, M.; Frederik, P. M.; Daemen, M. J.; van Engelshoven, J. M. Accumulation of ultrasmall superparamagnetic particles of iron oxide in human atherosclerotic plaques can be detected by *in vivo* magnetic resonance imaging. *Circulation* **2003**, *107*, 2453–2458.
98. Wu, Y. L.; Ye, Q.; Foley, L. M.; Hitchens, T. K.; Sato, K.; Williams, J. B.; Ho, C. In situ labeling of immune cells with iron oxide particles: an approach to detect organ rejection by cellular MRI. *Proc. Natl. Acad. Sci. U.S.A.* **2006**, *103*, 1852–1857.
99. Zimmer, C.; Wright, S. C., Jr; Engelhardt, R. T.; Johnson, G. A.; Kramm, C.; Breakefield, X. O.; Weissleder, R. Tumor cell endocytosis imaging facilitates delineation of the glioma–brain interface. *Exp. Neurol*. **1997**, *143*, 61–69.
100. Muldoon, L. L.; Sandor, M.; Pinkston, K. E.; Neuwelt, E. A. Imaging, distribution, and toxicity of superparamagnetic iron oxide magnetic resonance nanoparticles in the rat brain and intracerebral tumor. *Neurosurgery* **2005**, *57*, 785–796.
101. Brillet, P. Y.; Gazeau, F.; Luciani, A.; Bessoud, B.; Cuenod, C. A.; Siauve, N.; Pons, J. N.; Poupon, J.; Clément, O. Evaluation of tumoral enhancement by superparamagnetic iron oxide particles: comparative studies with ferumoxtran and anionic iron oxide nanoparticles. *Eur. Radiol*. **2005**, *15*, 1369–1377.
102. Fortin-Ripoche, J. P.; Martina, M. S.; Gazeau, F.; Menager, C.; Wilhelm, C.; Bacri, J. C.; Lesieur, S.; Clément, O. Magnetic targeting of magnetoliposomes to solid tumors with MR imaging monitoring in mice: feasibility. *Radiology* **2006**, *239*, 415–424.
103. Artemov, D.; Bhujwalla, Z. M.; Bulte, J. W. Magnetic resonance imaging of cell surface receptors using targeted contrast agents. *Curr. Pharm. Biotechnol*. **2004**, *5*, 485–494.
104. Hofmann, B.; Bogdanov, A.; Marecos, E.; Ebert, W.; Semmler, W.; Weissleder, R. Mechanism of gadophrin-2 accumulation in tumor necrosis. *J. Magn. Reson. Imaging* **1999**, *9*, 336–341.
105. Bulte, J. W. M.; In vivo MRI cell tracking: clinical studies. *AJR. Am. J. Roentgenol.* **2009**, *193*, 3314–3325.